ACS OMEGA

Article

Cite This: ACS Omega 2018, 3, 1304−1314

Transformation of Block Copolymer Nanoparticles from Ellipsoids with Striped Lamellae into Onionlike Spheres and Dynamical Control via Coupled Cahn−Hilliard Equations

Edgar Avalos,*,† Takashi Teramoto,*,§ Hideaki Komiyama,⊥ Hiroshi Yabu,*,⊥ and Yasumasa Nishiura*,‡

†Mathematical Science Group, WPI-Advanced Institute for Materials Research (AIMR), Tohoku University, 2-1-1 Katahira, Aoba-ku, Sendai, Miyagi 980-8577, Japan

‡Mathematical Science Group, WPI-Advanced Institute for Materials Research (AIMR), Tohoku University, MathAM-OIL, 2-1-1 Katahira, Aoba-ku, Sendai, Miyagi 980-8577, Japan

§Department of Mathematics, Asahikawa Medical University, 2-1-1-1, Midorigaoka-higashi, Asahikawa 078-8510, Japan

⊥Device/System Group, WPI-Advanced Institute for Materials Research (AIMR), Tohoku University, 2-1-1 Katahira, Aoba-ku, Sendai, Miyagi 980-8577, Japan

Supporting Information

ABSTRACT: Annealing of block copolymers has become a tool of great importance for the reconfiguration of nanoparticles. Here, we present the experimental results of annealing block copolymer nanoparticles and a theoretical model to describe the morphological transformation of ellipsoids with striped lamellae into onionlike spheres. A good correspondence between the experimental findings and predictions of the model was observed. The model based on finding the steepest direction of descent of an appropriate free energy leads to a set of Cahn−Hilliard equations that correctly describe the dynamical transformation of striped ellipsoids into onionlike spheres and reverse onionlike particles, regardless of the nature of the annealing process. This universality makes it possible to describe a variety of experimental conditions involving nanoparticles underlying a heating process. A notable advantage of the proposed approach is that it enables selective control of the interaction between the confined block copolymer and the surrounding medium. This feature endows the model with a great versatility to enable the reproduction of several combined effects of surfactants in diverse conditions, including cases with reverse affinities for the block copolymer segments. A phase diagram to describe a variety of morphologies is presented. We employ the relationship between the temperature-dependent Flory−Huggins parameter and the width of the interfaces to account for changes in temperature due to the heating process. Simulation results correctly show how the transformation evolves as the temperature increases. This increment in temperature corresponds to progressively smaller values of the interfacial width. We anticipate that the proposed approach will facilitate the design and more precise control of experiments involving various kinds of annealing processes.

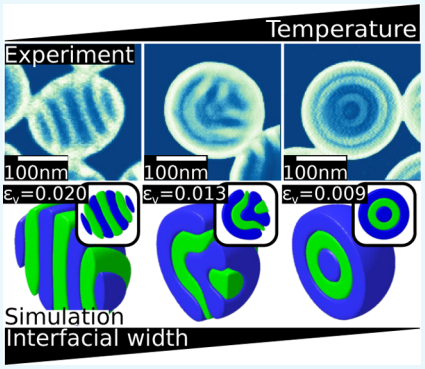

1. INTRODUCTION

Fine-tuning the individual structures of the building blocks in nanomaterials enables the function and properties of polymeric materials to be controlled.[1] Other fields as diverse as colloids[2] and lyotropic liquid crystals,[3] among others, also strive to gain a deep understanding of the changes in the shape and structure of the constitutive elements to gain precise control of the self-assembly processes.[4] In live systems, transformations during self-assembly often involve profound changes in symmetry, such as those observed in the gastrulation phase in early embryonic development.[5−7]

For inorganic materials, it is possible to tune the synthesis parameters to control the shapes of the nanoparticles and obtain nanoparticles a few nanometers wide.[8,9] In the case of organic materials, morphological control is rapidly developing, and it is now possible to control the shape of domains of a similar scale.[10−16] The interest in the latter case is partially motivated by the desire to synthesize bioinspired materials with applications in drug delivery,[17−25] among others.[26−30]

There are several aspects that contribute to the self-assembly of block copolymer (BCP) nanoparticles. For instance, the symmetrical composition of polystyrene-*block*-polyisoprene (PS-*b*-PI) in solution often results in nanoparticles with a layered morphology,[12] whereas asymmetrical composition leads to a variety of configurations.[31−33] Furthermore, by controlling the interaction between the solvent and the segments of the BCP, it is possible to fine-tune the nanosurfaces.[34]

Annealing is commonly used to modify the orientation and symmetry of polymeric nanoparticles.[35,36] Common types of annealing include thermal annealing and solvent annealing.

Received: October 15, 2017
Accepted: December 26, 2017
Published: January 31, 2018

DOI: 10.1021/acsomega.7b01557
ACS Omega 2018, 3, 1304−1314

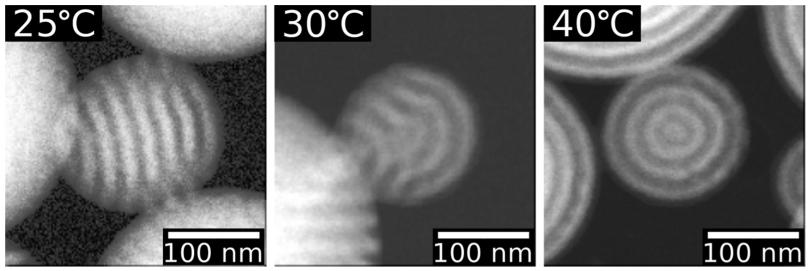

Figure 1. STEM images of PS-*b*-PI at different stages of the morphological transformation of a striped ellipsoid into an onionlike particle using annealing in water at different temperatures. From left to right, 25, 30, and 40 °C. As the temperature increases, the layers curl up to allow the polymer segments with more preference for water to maximize their contact with the surrounding medium, and at higher temperatures, only the PI segments are exposed to water. At 40 °C, the outermost layer of the onion particle is composed of PI segments. M_n (PS) = 17.8 kg/mol and M_n (PI) = 12.0 kg/mol. PI segments are stained with OsO_4 to brighten them in the STEM images.

Surfactant addition is another method that influences the morphology and shape of the particles by modifying the interfacial interaction between the BCP and the surrounding medium.

Thermal annealing directly employs heat to bring BCP nanoparticles to a certain temperature to induce an order−order phase transition in the material.[37,38] Cavicchi and Russell developed a technique that involved exposing the polymer to vapor of a good solvent, and they managed to complete the annealing process within 1 h.[39] The transformation time can be considerably reduced from several weeks to a few minutes by using microwaves as a source of heat.[38,40,41] Because it is desirable to carry out experiments in a short amount of time, this method is a notable contribution.

The addition of a surfactant also facilitates changes in the shape and internal morphology of BCPs. Notable examples involve the inclusion of gold nanoparticles to induce elaborate transformations of the BCP from a spherical to a lens shape[42] or to a striped ellipsoidal particle.[43] Temperature-responsive surfactants allow the production of ellipsoidal and convex lens BCP particles when polymer droplets are stabilized at high and low temperatures, respectively.[44] In another example of using surfactants to tune the interfacial properties of the BCP particles, a dramatic morphological transition from spherical to convex lens-shaped BCP particles was observed when the aspect ratio of CuPt nanorod surfactants was changed.[45] Using a mixture of surfactants, the morphologies can be transformed from onionlike to striped ellipsoidal particles[46,47] and striped ellipsoids into nanosheets with a hexagonal structure of homopolymer cylinders.[48] In another case, when using mixtures of various compositions of the two surfactants, an even richer variety of morphologies resulted: onionlike particles, ellipsoids with striped lamellae, and reverse onions. In the first and last cases, one component of the mixture of surfactants dominates, whereas in the layered case, both components balance one another.[49] One more example of exquisite crafting comes from a study in which 10 nm-sized graphene quantum dots behave as surfactants with tunable properties to produce nanoparticles of different shapes: spheres, reverse spheres, and convex lens.[50]

Taking the solvent parameters into consideration provides another method of creating intricate nanoparticle morphologies (solvent annealing).[51,52] Li et al. showed that one can use controlled precipitation from the good/poor solvent mixture to modulate the swelling and annealing of nanoparticles suspended in aqueous media.[53] Furthermore, in a different setting, it has been shown that solvent-induced reconfiguration processing of onionlike nanoparticles in ethanol produces selective swelling, and one must consider three factors: size, nanostructure, and the composition of the BCP. These factors intertwine to control the swelling behavior of the nanoparticles.[54] By using the process of solvent annealing, it is possible to produce reversible morphologies when combining the adsorption of chloroform and controlling the concentration of polyvinyl alcohol.[55] Another aspect that plays a significant role in the configuration of BCP is the rate at which the solvent evaporates. Rapid evaporation results in a layered morphology, but a slow rate allows only one of the segments in the BCP to reach the outermost layer because of the preferential interaction of the segment with the external matrix.[56] Another remarkable feature of the process of solvent annealing is that an inorganic precursor can be used to modify the morphology and shape of nanoparticles.[57] A common trend among several of the morphological transformations mentioned so far involves the structural changes of ellipsoids with striped lamellae into onionlike spheres. These changes in shape can also be found in other systems.[3,58]

Despite the large number of situations in which the transformation of striped ellipsoids into onionlike spheres appears, along with several techniques that have been developed to anneal nanoparticles, little effort has been made to understand the transformation process from an energy point of view.[59] In this work, we present a model based on an energy functional with short- and long-range contributions to describe this transformation. An appropriate minimization scheme of this energy functional leads to a set of Cahn−Hilliard equations that correctly describe the experimental results of thermal annealing.

Although Cahn−Hilliard equations are based on a small number of parameters, they provide a robust qualitative model to predict many kinds of possible morphologies and offer a guideline on how confined BCPs behave dynamically when the parameters are changed, regardless of the specifics of the annealing method employed.[34,60,61] For a wide range of processes involving the heating of BCPs in solution, this model establishes a clear parameter correspondence between, for instance, the temperature-dependent Flory−Huggins parameter and the width of the interface of the microphases. The universality of the model serves as a theoretical basis to design and perform experiments.

We have organized this paper as follows. We begin by describing a series of experimental settings for annealing in water and microwave annealing, followed by a description of the model with a particular emphasis on how the parameters of the model are related to the experimental quantities. The

DOI: 10.1021/acsomega.7b01557
ACS Omega 2018, 3, 1304−1314

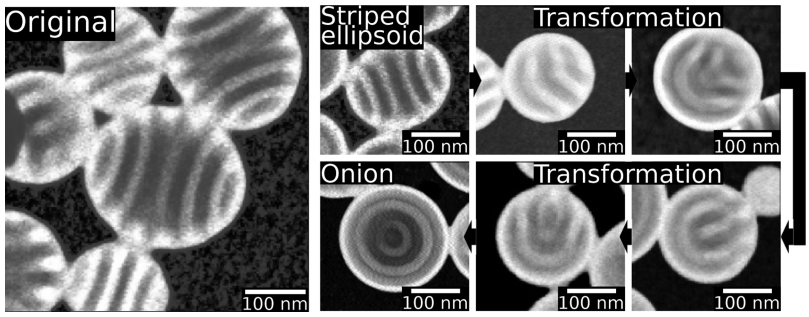

Figure 2. STEM images of PS-*b*-PI to show different stages of the morphological transformation of a striped ellipsoid into an onionlike particle using microwave annealing from 60 to 90 °C. Microwave annealing allows the morphological transformation to be completed within a few minutes, whereas conventional thermal annealing requires several days to complete the transformation. As the temperature increases, several stages of the transformation develop, namely, striped ellipsoid, semionion, and onion. The semionion stage has a number of substages in which some layers are partially exposed to the surrounding medium. At higher temperatures, only the outermost layer is exposed to water. M_n (PS) = 135 kg/mol and M_n (PI) = 131 kg/mol. PI segments are stained with OsO_4 to brighten them in the STEM images.

dependence on temperature is explained, and the numerical details are also addressed. A corresponding phase diagram is introduced afterward, along with a discussion on the transformation of a striped ellipsoid into an onionlike sphere and reverse onion morphology. We present our conclusions at the end.

2. RESULTS AND DISCUSSION

2.1. Experimental Results. *2.1.1. Water Annealing.* Figure 1 shows a sequence of samples at different temperatures to illustrate the transformation of a striped ellipsoid into an onionlike morphology in PS-*b*-PI nanoparticles produced by annealing in water. The dispersions were kept for two weeks. At low and high temperatures (25 and 40 °C), particles exhibit unidirectional stacked layer and onionlike morphologies, respectively. The transformation also has an intermediate stage at 30 °C, in which the particle has a semionion morphology. To understand this transformation, we recall that at a low temperature, the segments of the BCP PS-*b*-PI interact with similar strength with the solvent; thus, both components are equally able to reach the surface. This leads to the formation of particles with layered structures.

To offer some insight into how the interaction between copolymer segments changes with temperature, we measured the interfacial tensions between water and PS (57.9 mN/m) and between water and PI (55.8 mN/m). The measured values indicate that the PI segments have a slightly higher preference for the water phase. Although it is challenging to obtain precise measurements of the contact angles and interfacial tensions at variable temperatures using the present equipment, the Flory–Huggins theory states that the free energy of a mixture increases linearly with increasing temperatures. It is therefore reasonable to expect higher interfacial tension values at higher temperatures. The upshot is that increasing the temperature leads to reduced values of the Flory–Huggins parameter, making water a better solvent for the PI segments. This in turn facilitates the interaction of these segments with the solvent, and thus, the PI segments will be more likely to reach the surface of the particles. These particles will be characterized by an onionlike structure with their preferential outermost layer in contact with the solvent. In section 2.5, it will be shown that onionlike morphologies are energetically stable.[34]

Another relevant aspect to consider is the effect of the particle size on the transformation process. It has been previously reported that particles smaller than 200 nm rapidly evolve from a disordered state into an onionlike morphology, whereas larger particles remain unchanged even after annealing at 30 °C for two weeks.[37,38] Nevertheless, this initially stiff structure of a striped ellipsoid was eventually transformed into an onionlike sphere after annealing at 40 °C for two weeks.

2.1.2. Microwave Annealing. Annealing time, in general, decreases at high temperatures. One of the greatest advantages of microwave annealing over water annealing is a reduction in the processing time from weeks to several minutes. Figure 2 shows the different stages of microwave annealing for the transformation of striped ellipsoids into onionlike particles. In the experiments, when the nanoparticle dispersion was annealed at 60 °C, the transformation into onionlike particles required about 60 min.[38] At the slightly higher temperature of 70 °C, at each point in time, we observed the following ordered structures. First, unidirectionally stacked layered structures and then transformed layered structures were formed in the nanoparticles after annealing for 5 min. After 25 min, semionion and onionlike structures were observed in the nanoparticles. In contrast, annealing at 90 °C resulted in the formation of the onionlike structures after only 5 min.

An explanation of the notable reduction in the processing time is in order. Microwaves provide a fast and uniform heating mechanism, and although the dielectric constant of the polymers is low, they still partially absorb a small amount of radiation, providing extra molecular motion to the polymer segment with a preferential interaction toward water. Thus, the segment with preferential interactions reaches the surface of the particle to form an onionlike morphology. Despite the fact that a systematic study to analyze the effect of temperature on the interaction of each polymer segment with water is still pending, it is reasonable to expect that the transformation will take place at a faster rate if the polymer segment has a higher affinity for water. The results of water and microwave annealing presented in this work exhibit identical features of the morphological transformation of striped ellipsoids into onionlike spheres shown in electron tomography observations previously reported.[37]

2.2. Theoretical Model. *2.2.1. Dynamical Equations.* In the following theoretical model, we assume that a BCP particle is immersed in an external medium, which could be a homopolymer, a solvent, or water, for instance. Hereafter, without the loss of generality of the model, we refer to the external medium as the homopolymer.[62] This model for the mixture of two systems has been previously described.[34] The

DOI: 10.1021/acsomega.7b01557
ACS Omega 2018, 3, 1304–1314

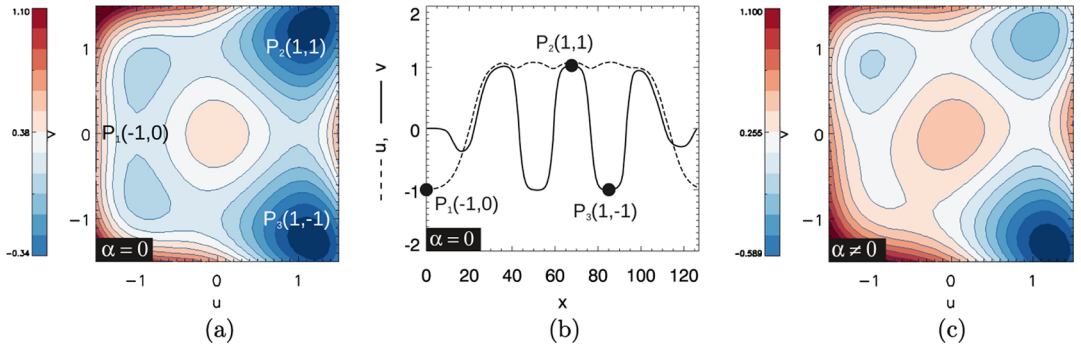

Figure 3. (a) Energy contour plot of $W(u, v)$ in eq 2 with $\alpha = 0$ (symmetric plot). In this case, u has equal preference for $v < 0$ or $v > 0$. P_1, P_2, and P_3 are locations where (u, v) are, respectively, $(-1, 0)$, $(1, 1)$, and $(1, -1)$. P_2 and P_3 are located at the boundary within which a particle is confined. (b) Schematic figure of the confined particle in one dimension. This is the case of $\alpha = 0$, where the confining surface has equal preference for $v < 0$ or $v > 0$. Notice that the confining surface defined by v is not rigid, but rather it adopts the undulations of v at the surface of the particle. (c) Energy contour plot of $W(u, v)$ with $\alpha \neq 0$ (asymmetric plot). In this case, u has different preference for $v < 0$ or $v > 0$.

morphologies consist of two main components, namely, a confinement surface to keep a particle located in a section of the spatial domain and a BCP component within the surface, which undergoes phase separation.

The first component in the mixture is a blend of the homopolymer or water and an AB-type BCP. This component is described by order parameter u, and it acquires values within the interval $[-1, 1]$, with the end points of the interval corresponding to the homopolymer-rich domain (-1) and the BCP-rich domain $(+1)$. The boundary between the homopolymer and the BCP domains defines the boundary of the BCP particles. The second component is described by order parameter v, which defines the state of the AB-type BCP, and it also acquires values from the interval $[-1, 1]$, with the end points corresponding to A and B, respectively.

When the two systems mentioned above interact with one another, a macrophase separation described by u generates a region in which a BCP particle will be located and surrounded by the homopolymer. A microphase separation then takes place inside the separated BCP domain, which in turn is described by v. The dynamics of the state of these two mixed systems evolves to minimize the value of an energy functional as in the following expression

$$F \equiv F_{\epsilon_u, \epsilon_v, \sigma}(u, v) = \int_\Omega \left\{ \frac{\epsilon_u^2}{2} |\nabla u|^2 + \frac{\epsilon_v^2}{2} |\nabla v|^2 + W(u, v) + \frac{\sigma}{2} |(-\Delta)^{-1/2}(v - \bar{v})|^2 \right\} dr \quad (1)$$

where

$$W(u, v) = \frac{(u^2 - 1)^2}{4} + \frac{(v^2 - 1)^2}{4} + \alpha uv + \beta uv^2 + \gamma u^2 v \quad (2)$$

In eq 1, Ω is a smooth bounded domain in R^N. Here, we focus on the three-dimensional confinement and thus $N = 3$. Parameters ϵ_u and ϵ_v are proportional to the thickness of the propagating fronts of each component. These parameters control the size of the interface between the macrophase and the microphase. $\bar{v}$ is the mass ratio between two polymers. We set $\sigma \neq 0$ to turn on the long-range interactions in eq 1 that are needed to obtain particles with a fine structure, such as striped ellipsoids or onionlike spheres. To represent the long-range interactions in the original formulation of the energy functional for a problem with one component, Ohta and Kawasaki[59,63] used Green functions. Nishiura and Ohnishi[64] introduced an elegant formulation using the fractional power of the Laplace operator, which is more suitable for variational problems. Unlike the local operator ∇, which considers only interactions between neighboring positions, the nonlocal operator $(-\Delta)^{-1/2}$ must be evaluated over the entire domain Ω to correctly account for the long-range interactions related to σ.

The double-well potential in eq 2 represents two different possible states in a phase transition, -1 or $+1$. This function has two dimensions and coupling parameters α, β, and γ. We set $\gamma = 0$.

The coupling parameter α causes symmetry breaking between the microphase-separated domains, and by changing its value, we can control the interaction between the confining surface and the confined BCP. To understand how the coupling parameter α affects the confined morphologies, Figure 3 shows contour plots of $W(u, v)$ for different values of α. If $\alpha = 0$, the contour lines in Figure 3a are symmetrical, which indicates that u has equal preference for any value of v, either positive or negative. For instance, in the case of a layered morphology, both positive and negative values of v of the particle are equally able to reach the confining surface because $\alpha = 0$. Conversely, if $\alpha \neq 0$, then the contour plot is asymmetrical, as shown in Figure 3c, and thus the preference of u for v depends on whether v is positive or negative. $\alpha \neq 0$ would be appropriate to simulate a confining surface with more preference for one of the BCP segments, as in the case of onionlike particles among others. The coupling parameter β affects the free energy depending on the value of u, as $v^2 > 0$. For most of the cases presented here, $\bar{u} < 0$, and thus the energy term involving β in eq 2 raises or lowers the double well when $\beta < 0$ or $\beta > 0$, respectively.

The associated Euler–Lagrange system of equations corresponding to the mixed system comprises two coupled Cahn–Hilliard equations, as follows

$$\tau_u u_t = \Delta\left(\frac{\delta F}{\delta u}\right) \quad (3)$$

$$= -\Delta\{\epsilon_u^2 \Delta u + (1 - u)(1 + u)u - \alpha v - \beta v^2\} \quad (4)$$

DOI: 10.1021/acsomega.7b01557
ACS Omega 2018, 3, 1304−1314

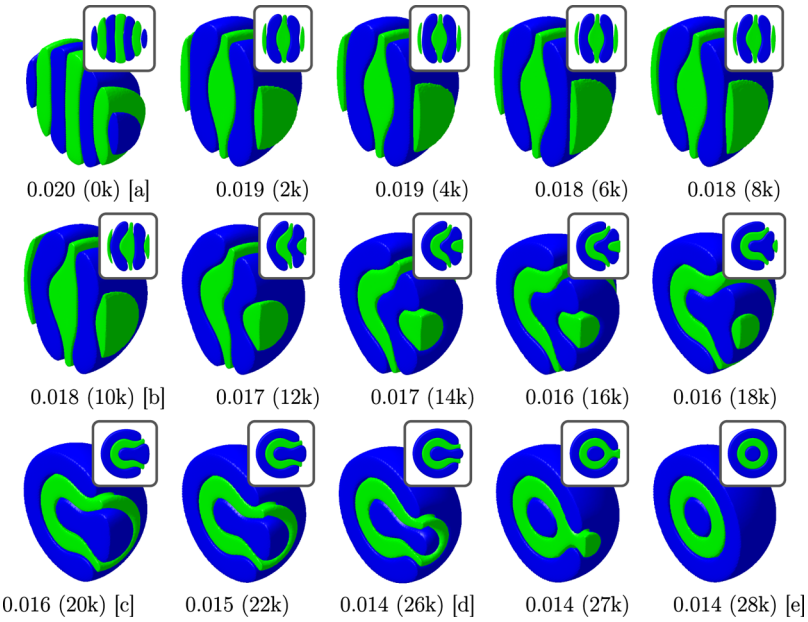

Figure 4. Changes in morphology during the transformation of an ellipsoid with striped lamellae into an onionlike sphere for $\alpha = 0.3$. Half-section views of three-dimensional isosurfaces with an inclination about the z-axis are shown to make the internal features of the transformation visible. Insets: Cross sections of the morphologies. Isosurfaces at an appropriate threshold are shown for the order parameter $v < 0$ (blue) and $v > 0$ (green). Values of the interfacial width, ϵ_v, are shown in each case along with the cumulative number of time steps (in parenthesis). Projections onto the x-axis of order parameters u and v during the morphological transformation are shown in Figure 5. We select stages [a–e] to analyze the evolution of the energy of the transformation (see Figure 8).

$$\tau_v v_t = \Delta\left(\frac{\delta F}{\delta v}\right) \tag{5}$$

$$= -\Delta\{\epsilon_v^2 \Delta v + (1 - v)(1 + v)v - \alpha u - 2\beta uv\} - \sigma(v - \bar{v}) \tag{6}$$

F is defined in eq 1, and parameters τ_u and τ_v are time constants to control the speed at which parameters u and v move. Equations 4 and 6 constitute a mixture of two coexisting systems: one with $\sigma = 0$ and the other with $\sigma \neq 0$. The former separates a confined BCP nanoparticle from the surrounding external medium, and the latter system with $\sigma \neq 0$ allows the nanoparticle to form microphases. The parameter α controls the affinity of the surrounding medium for the confined particle in such a way that as α increases, the preference for a BCP segment increases accordingly. The proposed approach allows the problem to be solved by integrating a set of equations for the whole system, thus avoiding the explicit treatment of the boundary conditions at the interface between the BCP and homopolymer domains.

2.2.2. How the Temperature-Dependent Flory–Huggins Parameter Relates to the Interface Width. To account for thermal changes during the annealing process, we need to relate the dynamical evolution of the state of the system to changes in temperature. Equations 4 and 6 correctly describe the time evolution of the order parameters u and v. Although these equations are not explicitly temperature-dependent, it is known that the interfacial width between BCP segments diminishes with the temperature-dependent Flory–Huggins interaction parameter, χ_{AB}, as follows (see refs 65 and 66)

$$\epsilon_v = \frac{2a}{\sqrt{6\chi_{AB}}} \tag{7}$$

Moreover, the effective value of χ_{AB} increases with temperature as follows (see refs 67 and 68)

$$\chi_{AB} = \frac{(\chi_{AB} - \chi_{BS})^2}{(\delta_A - \delta_B - 2\delta_S)^2}\frac{RT}{\nu} \tag{8}$$

where χ_{AS} and χ_{BS} correspond to polymer A with solvent and polymer B with solvent, respectively. R is the universal gas constant, T is the temperature, ν is the molar volume, and δ is the solubility parameter. If one of the segments in the BCP has more preference for the solvent, then $(\chi_{AS} - \chi_{BS})^2$ enlarges χ_{AB}, which in turn leads to a reduction in the value of the interfacial width, $\epsilon_v \propto 1/T^{1/2}$. The approach that we use consists of dividing the process of thermal annealing into a sequence of stages, each one at a constant temperature (constant ϵ_v). At each stage, eqs 4 and 6 are valid, and we can correctly account for the heating process.

Because of technical limitations, it is extremely demanding to obtain direct measurements of the interfacial thicknesses of the phases formed in the particles. On the other hand, Helfand and Tagami[65,66] proved—theoretically and experimentally—that there is a robust relationship between the variations in temperature and the changes in the interfacial thickness of a polymer in bulk. We rely on these relationships to develop our model, and it will be shown that this model successfully reproduces the experimental results in BCP particles.

2.3. Simulation of Annealing of Nanoparticles. Here, we describe the simulation of the annealing process. First, we need to select a suitable initial condition at an appropriate initial temperature in a cubic lattice. Because at room temperature the external medium has equal preference for any segment of the BCP, the initial condition should be a particle with unidirectionally stacked lamellae (striped ellipsoid) with $\alpha = 0$. When the parameter responsible for the affinity of the external medium for the segments of the BCP

DOI: 10.1021/acsomega.7b01557
ACS Omega 2018, 3, 1304–1314

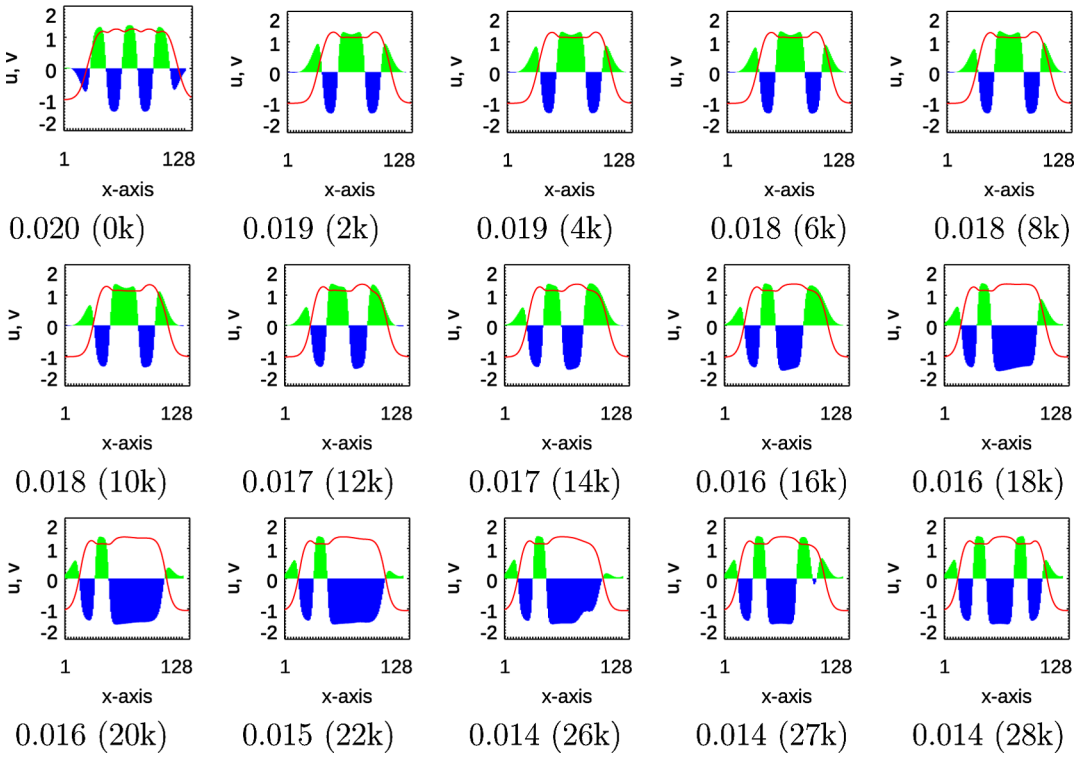

Figure 5. Projection onto the x-axis of order parameters u and v during the morphological transformation of an ellipsoid with striped lamellae into an onionlike sphere for $\alpha = 0.3$. The order parameter u is depicted in red, and v is represented as a histogram of intensities. The size of the bar represents the magnitude of v along the x-axis. Green bars correspond to $v > 0$, and blue bars correspond to $v < 0$. Values of ϵ_v are shown in each case along with the cumulative number of time steps (in parenthesis). Each profile in this figure corresponds to the stages shown in Figure 4.

is set to zero, the corresponding contour plot of the energy is symmetrical, as shown in the contour plot in Figure 3a. Now, we proceed to select an initial value for the temperature of the striped ellipsoid. According to eqs 7 and 8, the temperature is related to the width of the interface as $T \propto 1/\epsilon_v^2$. A reasonable choice for the interface width of a typical striped ellipsoid is $\epsilon_v = 0.020$, and we progressively decrease this value until we reach a desired lower limit, corresponding to a final upper temperature. We perform this scheme for different values of α.

We start with $\alpha = 0$ for the simplest case of annealing. In this case, the interfacial width diminishes as the temperature rises, and this narrowing of the interface results in more room available for the formation of additional layers. In other words, in this case, the total number of stacked layers in the particle increases during the heating process, although the striped ellipsoid does not transform into an onionlike particle. To analyze the effect of the strength of the interaction with the external medium, the symmetry of the energy contour in Figure 3a must be broken up by selecting nonzero values for α. We select the following values to simulate a moderate preference of the external matrix for one of the BCP segments: $\alpha = 0.23$, 0.25, 0.27, and 0.3. Smaller values of α seem to be insufficient to complete the morphological transformation, and the values of $\alpha > 0.3$ correspond to different experimental parameters.

We simulate annealing while keeping a record of the changes in morphology for different values of α. Then, we use this information to analyze the relationship between α and the dynamic morphological changes.

Figure 4 shows several stages during the morphological transformation for $\alpha = 0.3$. During the transformation, order parameters u and v vary accordingly in a complicated manner. However, we can appreciate how these parameters are intertwined by considering their projection onto a direction that is parallel to the main axis of the particle. Figure 5 illustrates how u and v vary in time and space, as seen in one of the three spatial dimensions of the domain. Notice that the order parameter u remains mostly unchanged during the transformation because its main role is to establish a boundary for the particle, and the particle remains confined during the process. On the contrary, the order parameter v undergoes profound changes in its distribution within the body of the particle, which is why the variations in v are more noticeable than those of u. Naturally, the evolution of u and v will look different when projected in different directions.

The transformation process for moderate values of α is similar, with the notable difference that the transformation develops faster for larger values of α, which is expected because a strong preference for a BCP segment facilitates the transformation process. To account for the duration of the transformation, we define the completion time t_c as the total time required for the initial striped ellipsoid to complete the transformation into a closed onionlike particle. As an example, for $\alpha = 0.23$ and $\alpha = 0.30$, the onion is complete at $t_c = 47\,000$ time steps (at $\epsilon_v = 0.010$) and $t_c = 28\,000$ time steps (at $\epsilon_v = 0.014$), respectively. Figure 6 shows that t_c diminishes with α and that once the transformation process is complete, the final state is a steady onionlike morphology.

2.4. Phase Diagram of Transformed Morphologies.

Figure 7 shows a phase diagram to illustrate the various morphologies obtained in the previous section. The diagram describes the morphologies resulting from annealing at different values of α. For each value of α, the heating process starts at a given temperature, which in turn depends on the interface width as $T \propto 1/\epsilon_v^2$.

DOI: 10.1021/acsomega.7b01557
ACS Omega 2018, 3, 1304−1314

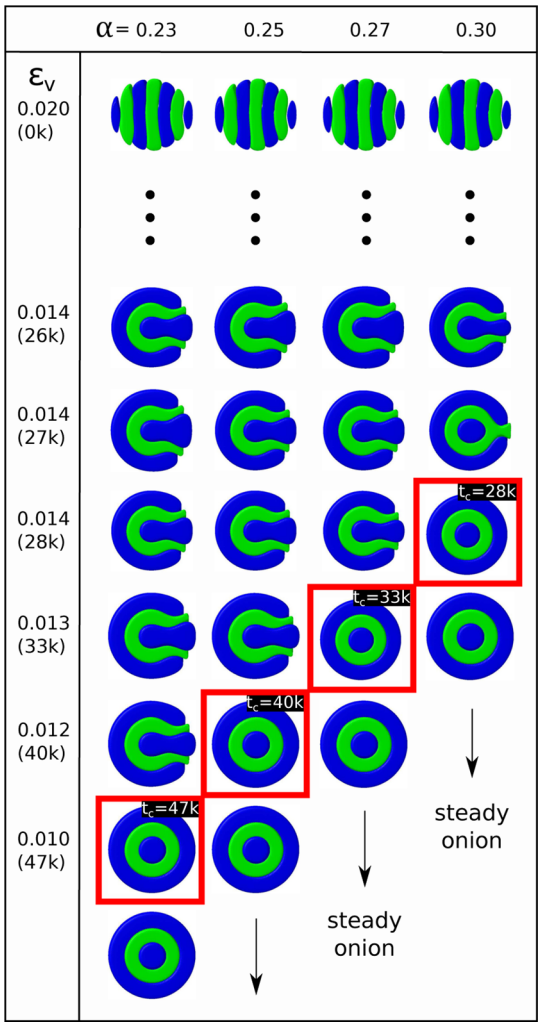

Figure 6. Transformation of ellipsoids with striped lamellae to onionlike spheres for progressively increasing the values of α (left to right). Top to bottom: Cross sections of the three-dimensional morphology taken at different times to show the transformation in detail. The simulation starts from a common initial condition shown at the top and then the interface width, ϵ_v, decreases progressively. Values of ϵ_v are shown on the y-axis from top to bottom with the cumulative number of time steps (in parenthesis). The order parameter ν is shown in blue for $\nu < 0$ and green for $\nu > 0$. The transformation is completed after a period of time t_c has passed (highlighted for each value of α). In this region of parameters, t_c decreases with α. Full details of the transformation for $\alpha = 0.3$ are shown in Figure 4.

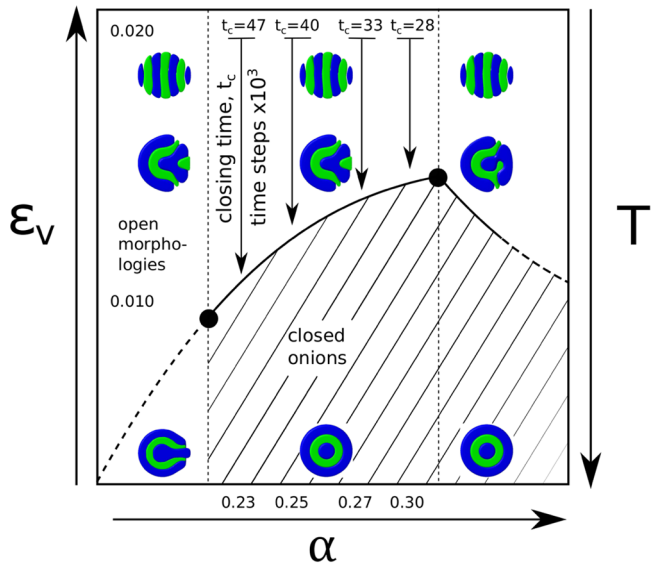

Figure 7. Phase diagram of the morphologies found in simulations for different values of ϵ_v and α. The right y-axis represents the temperature, $T \propto 1/\epsilon_v^2$. The region between the vertical dashed lines represents the results of transformations of ellipsoids with striped lamellae to onionlike spheres, similar to what is found in the experiments. The transformation process starts with a layered morphology at $\epsilon_v = 0.020$, and this value becomes smaller as the transformation progresses. The transformation is complete after a period of time t_c has passed, and a typical final result is shown in the area between vertical dashed lines of the closed onionlike morphologies. In this region, closing time, t_c, decreases with α. Some representative stages of the transformation are shown in the diagram. The order parameter ν is shown in blue for $\nu < 0$ and green for $\nu > 0$.

The simplest case is $\alpha = 0$. In this case, the interfacial width diminishes when the temperature rises, and this narrowing of the interface results in more room being available for additional layers. However, in this case, the striped ellipsoid does not transform into an onionlike sphere.

Now, we consider cases with $\alpha \neq 0$ and probe the parameter space with a unidirectionally layered morphology. On the left-hand side of the phase diagram, there is a region of small values of α for which the affinity for the BCP segments is not very strong. In this region, although the inner layers of the striped ellipsoid partially curl up around the core, the external layers are unable to form closed surfaces. In this case, the morphology remains open, even at high temperatures.

When the value of $\alpha > 0$ is barely larger than the threshold value, we enter into a region in which the preference for the external medium is large enough to conduct a complete transformation from a striped ellipsoid into an onionlike sphere. Within this region, layers curl up to form onionlike shapes when we increase the temperature, although for small values of α, the annealing of particles will be slow and thus, the onions will take a long time to close their external layer. As we increase the value of α, the preference for the solvent increases accordingly, resulting in a reduction in the annealing time. The transformation of a striped ellipsoid into an onionlike sphere is still possible after an upper limit of the value of α has been reached, although the intermediate stages in this case appear to be significantly different in their inner morphology than those in the cases with smaller α values, and they evolve at different speeds. Morphologies with large values of α are in the region on the right-hand side of the vertical dashed line at $\alpha > 0.30$ in the phase diagram in Figure 7. The curve with a positive derivative in the figure represents a border numerically found that separates the temperature at which the morphology closes its outermost external layer.

During experiments, it is more common to observe transformations within the region between the dashed lines in the phase diagram in Figure 7. This behavior can be explained by the fact that both segments of the BCP used in the experiments have a similar affinity for the solvent; thus, the relative preference of the solvent for any of the two segments in the BCP is quite similar. This situation corresponds to moderate values of α. Values of $\alpha > 0.35$ would be appropriate for experimental conditions involving stronger differences in the affinity of the segments, and in such cases, it is reasonable

DOI: 10.1021/acsomega.7b01557
ACS Omega 2018, 3, 1304−1314

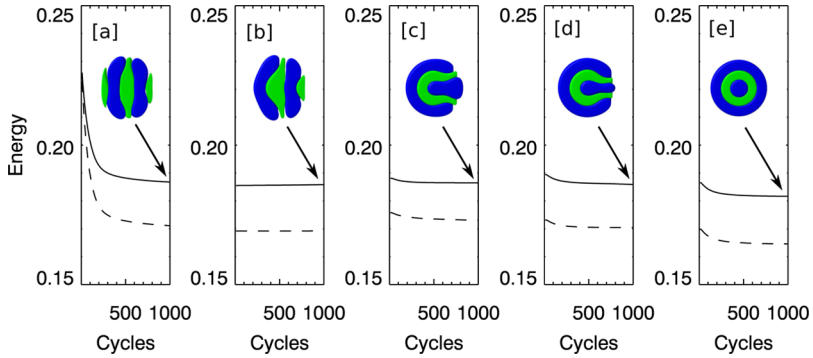

Figure 8. Evolution of the energy in the transformation of a system with $\alpha = 0.30$ (solid) and $\alpha = 0.35$ (dashed). To compare the energies of different stages at $\alpha = 0.30$, we placed the morphologies shown in stages [a−e] in Figure 4 in a common parameter space with $\epsilon_\nu = 0.018$ and then let the system evolve for another 1000 time steps. The insets in each panel show cross sections of the morphology obtained at the end of 1000 time steps. The order parameter ν is shown in blue for $\nu < 0$ and green for $\nu > 0$. The arrows indicate the time at which the morphology was complete. The decreasing values of the energy show that the system evolves toward a more stable state during the transformation of a striped ellipsoid into an onionlike sphere.

to expect a transformation from a striped ellipsoid into an onionlike sphere with intermediate stages resembling a particle with intertwined layers at the core.

2.5. Energy of the Transformation. In this section, we proceed to analyze the energy of the transformation. Figure 8 shows the evolution of the energy during the transformation as the total sum in the energy functional in eq 1. During the simulation of annealing, we progressively decrease ϵ_ν, altering the energy content of the abovementioned functional, and the upshot is that each stage of the process has a different energy value. To compare the energy at different stages of the transformation, first we need to adjust the resulting morphologies to have common values of the parameter ϵ_ν and then let the system evolve for a period of time. We perform this operation in several stages for the cases with $\alpha = 0.30$ and $\alpha = 0.35$. The first case corresponds to the transformation observed in Figure 4, which is the fastest case that exhibits natural bending of the layers, similar to that observed in the experiments. The second case corresponds to a transition in which the bending of the layers is more pronounced because it causes the inner layers to curl up and intertwine with one another (not shown here). Nonetheless, the end result is also closed onions. Figure 8 shows both cases of α and demonstrates that the general tendency is toward lower values of energy, which is expected because onions are typically one of the most stable morphologies. It is necessary to stress that Figure 8 does not represent the evolution of the transformation shown in Figure 4 because in the latter case, the interface width of the morphology progressively dwindles. In contrast, in Figure 8, the interface is kept constant throughout the simulation time.

To additionally verify the robustness of the final onionlike state, we simulated the reverse process. We started the dynamics from an onionlike morphology state and progressively increased the value of ϵ_ν to a value corresponding to a striped ellipsoid, while keeping all the other parameters unchanged. Our results suggest that the final onionlike state is quite robust as this morphology remained unchanged for over 40 000 time steps. This further confirms the experimental finding that the nanoparticles transform irreversibly into onionlike particles.

2.6. Reverse Onionlike Particles. In this section, we further expand the applications of our model. Klinger et al. have used a mixture of two surfactants in solution with a BCP, in such a way that one surfactant has more affinity for one segment of the polymer, whereas the other surfactant has more affinity for the other segment.[49] The authors could control the relative mass fraction of one surfactant with respect to that of the other surfactant, and by adjusting the composition of the mixture, they could obtain particles with reverse morphologies.

This raises the question of whether it is possible to reproduce the results of the described experiment. Although in this setting there are two competing components playing the role of the homopolymer, and considering that these two components have opposite effects, our model can be used to effectively reproduce the effect of the mixture of the two surfactants by switching the sign of the parameter α, which is responsible for the interaction between the BCP and the homopolymer. When the mass fraction of one surfactant is dominant, we use $\alpha > 0$, and when the other surfactant is dominant, then $\alpha < 0$. When the contributions of both surfactants balance one another, we use $\alpha = 0$.

In the numerical simulations, to realize the transformation of an ellipsoid into an onionlike sphere, we start with an initial condition with a unidirectionally stacked layered structure and select an external matrix with $\alpha > 0$. Conversely, we select $\alpha < 0$ to obtain a reverse onionlike morphology. A comparison of cases with $\alpha > 0$ and $\alpha < 0$ can be found in the Supporting Information for this work.

3. CONCLUSIONS

We have presented experimental and numerical results of thermal annealing of BCP nanoparticles and managed to correctly reproduce the outcomes of experiments of annealing in water and microwave annealing of particles 100 nm in diameter. The strength of our work is that the proposed model describes the dynamics and the outcome of diverse annealing processes in BCPs excellently, regardless of the particular annealing technique used. The model is based on an energy functional with short- and long-range contributions. Coupled Cahn−Hilliard equations are used to describe the morphological transformations of striped ellipsoids into onionlike forms, as seen in nanoparticles undergoing an annealing process. To account for changes in the temperature, we focused on the relationship between the temperature-dependent Flory−Huggins parameter and the thickness of the interface, suggesting that $T \propto 1/\epsilon_\nu^2$. A corresponding phase

DOI: 10.1021/acsomega.7b01557
ACS Omega 2018, 3, 1304−1314

diagram of the morphologies was presented. Both ellipsoids with striped lamellae and onionlike morphologies are energetically stable, although onions are typically in a lower position in the phase diagram of the energies of small particles.[34] We have discussed how to relate the experimental parameters of the annealing process to the simulation parameters of the transformation of striped ellipsoids into onionlike spheres and found that the speed of the process strongly depends on the affinity of the external matrix for the segments of the BCP. The net effect of increasing α is a reduction of the maximum annealing temperature. The present findings might help to establish a firm theoretical basis that can be applied to the design of experiments on annealing.

Furthermore, we have presented a scheme to produce onionlike and reverse onionlike morphologies and discovered that for $\alpha > 0$, it is possible to anneal lamellae particles regardless of the ordering of layers. However, in some cases of $\alpha < 0$, a full transformation is possible only if the ending caps of the particles have values of $\nu > 0$. This brings an intriguing possibility that might be tested in the future, which we describe as follows.

Higuchi et al. have shown that annealing in water produces a wide distribution of nanoparticles with striped ellipsoids and onionlike particles, the latter being the most numerous in the sample.[37] However, a number of striped ellipsoid particles remain unchanged. Experimentally, it is challenging to identify the caps of the particles and even more ambitious is to control the ordering of the layers in the nanoparticles. Our findings suggest that if the ordering of the caps in nanoparticles is controlled, it would enable a more precise outcome of the annealing process; thus, this area should be addressed in the future. Another area of research would address the annealing of large nanoparticles. Preliminary work suggests that adding thermal noise to large particles might be needed to facilitate the movement of local minimizers to reach a more stable state, similar to that found in experiments. These additional challenges should be addressed in forthcoming works.

4. METHODS

4.1. Preparation and Annealing in Water of Nanoparticles. The BCP composed of PS and PI segments with similar segment volumes of PS and PI was purchased from Polymer Source, Inc. (Dorval, Quebec, Canada). The molecular characteristics of this BCP are summarized in row one of Table 1. The BCP was dissolved in tetrahydrofuran (THF, with stabilizer, Wako Pure Chemical Industries, Ltd., Japan) to a final concentration of 0.1 g L^{-1}. Deionized water (2 mL) was then added to 1 mL of the BCP solution while stirring at 10 °C. Subsequently, THF was gradually evaporated at constant temperatures ranging from 10 to 40 °C over 2 days, and the BCP precipitated as nanoparticles in water.

Table 1. Molecular Characteristics of Polymers

name	M_n (PS) [g/mol]	M_n (PI) [g/mol]	M_w/M_n	f_{PI}
PS-*b*-PI-1	17 800	12 000	1.02	0.43
PS-*b*-PI-2	135 000	131 000	1.10	0.47

Annealing in water takes place once the solvent evaporation has been completed. The dispersion of nanoparticles is annealed with stepwise increments of the temperature for two weeks. At each temperature, the solution is sampled and then prepared for observation.

4.2. Microwave Annealing of Nanoparticles. Here, we used a PS-*b*-PI BCP purchased from Polymer Source, Inc. (Dorval, Quebec, Canada). The molecular characteristics are shown in row two of Table 1. The preparation of the BCP is similar to that for annealing in water, except that in this case, a rotary evaporator is used to accelerate the evaporation of THF. Subsequently, the BCP precipitates as nanoparticles.

To control the microwave annealing conditions, a microwave system was employed (Topwave; output power: 0−1000 W; frequency: 2.45 GHz; Analytik Jena, Germany), which can control the temperature and measure the pressure in the vessels. The nanoparticle dispersions were heated up to 90 °C for a time interval of up to 5 min and then maintained at that temperature for various holding times (5−60 min). After microwave annealing, the nanoparticle dispersions were gradually cooled to room temperature. Staining and preparation of the samples was performed as in the water-annealing experiments.

4.3. Scanning Transmission Electron Microscopy of Nanoparticles. Phase-separated structures in nanoparticles were observed by scanning transmission electron microscopy (STEM, HD-2000, Hitachi High-Technologies Corp., Japan) operated at 200 kV. To enable the PI segments to be visible in the STEM images, BCP nanoparticles were stained with OsO_4 for several hours. The stained nanoparticles were then redispersed in water with ultrasonication, and drops of the dispersion were placed onto Cu grids with elastic carbon membranes (Okenshoji Co., Ltd., Japan).

4.4. Computational Details. To integrate eqs 4 and 6, we implement a variation of the linear implicit scheme discussed previously in refs 69 and 70. To treat nonlinearities in these expressions, we split the cubic term into the product of a quadratic term related to the state of system at the first time step and a linear term related to the state of the system at next time step. This scheme is numerically stable and allows relatively large time steps ($\Delta t \approx 0.01$). The numerical solution of the coupled system of equations guarantees the production of morphologies of minimum free energy when the simulation time is long enough. Likewise, the solution of the Cahn−Hilliard equations ensures that the total volume $(1/|\Omega|)\int_\Omega \nu_0 \, dx^3$ remains constant, where ν_0 is the initial distribution of the BCP in the whole domain.

We select appropriate values of the parameters for the model presented above and then solve the dynamical equations. As a simulation cell, we use a cubic 128 × 128 × 128 lattice with periodic boundary conditions in the *x*-, *y*-, and *z*-axes of the lattice box. This size is appropriate for observing morphologies similar to those found in the experiments. To represent the three-dimensional morphologies, we plot isosurfaces taken at appropriate values of the order parameter ν.

■ ASSOCIATED CONTENT

Supporting Information

The Supporting Information is available free of charge on the ACS Publications website at DOI: 10.1021/acsomega.7b01557.

Details of the derivation of the theoretical model, simulation results for $\alpha = 0$, and cross sections of the nanoparticles during the transformation at different values of α (PDF)

DOI: 10.1021/acsomega.7b01557
ACS Omega 2018, 3, 1304−1314

AUTHOR INFORMATION

Corresponding Authors

*E-mail: avalos.hernandez.edgar.c2@tohoku.ac.jp (E.A.).
*E-mail: teramoto@asahikawa-med.ac.jp (T.T.).
*E-mail: hiroshi.yabu.d5@tohoku.ac.jp (H.Y.).
*E-mail: nishiura@tohoku.ac.jp (Y.N.).

ORCID

Edgar Avalos: 0000-0002-3009-6176

Notes

The authors declare no competing financial interest.

ACKNOWLEDGMENTS

E.A. and Y.N. gratefully acknowledge the support of Council for Science, Technology and Innovation (CSTI), Cross-ministerial Strategic Innovation Promotion Program (SIP), "Structural Materials for Innovation" (Funding agency: JST). T.T. acknowledges the use of the computer of the MEXT Joint Usage/Research Center "Center for Mathematical Modeling and Applications", Meiji Institute for Advanced Study of Mathematical Sciences (MIMS). This work was supported by JSPS A3 Foresight program and by JSPS KAKENHI grant nos. B26310205, 15KT0100, 26708025, 17H01223, 16K14701, and 16K21218.

REFERENCES

(1) Chen, C.; Wylie, R. A. L.; Klinger, D.; Connal, L. A. Shape Control of Soft Nanoparticles and Their Assemblies. *Chem. Mater.* **2017**, *29*, 1918−1945.
(2) Sacanna, S.; Korpics, M.; Rodriguez, K.; Colón-Meléndez, L.; Kim, S.-H.; Pine, D. J.; Yi, G.-R. Shaping colloids for self-assembly. *Nat. Commun.* **2013**, *4*, 1688.
(3) Iwashita, Y.; Tanaka, H. Spontaneous Onion-Structure Formation from Planar Lamellar Nuclei. *Phys. Rev. Lett.* **2007**, *98*, 145703.
(4) Gang, O.; Zhang, Y. Shaping Phases by Phasing Shapes. *ACS Nano* **2011**, *5*, 8459−8465.
(5) McClay, D. R.; Armstrong, N. A.; Hardin, J. Pattern formation during gastrulation in the sea urchin embryo. *Development* **1992**, *116*, 33−41.
(6) Wolpert, L. Gastrulation and the evolution of development. *Development* **1992**, *116*, 7−13.
(7) Vasiev, B.; Balter, A.; Chaplain, M.; Glazier, J. A.; Weijer, C. J. Modeling Gastrulation in the Chick Embryo: Formation of the Primitive Streak. *PLoS One* **2010**, *5*, No. e10571.
(8) Gou, L.; Murphy, C. J. Fine-Tuning the Shape of Gold Nanorods. *Chem. Mater.* **2005**, *17*, 3668−3672.
(9) Sau, T. K.; Rogach, A. L. Nonspherical Noble Metal Nanoparticles: Colloid-Chemical Synthesis and Morphology Control. *Adv. Mater.* **2010**, *22*, 1781−1804.
(10) Champion, J. A.; Katare, Y. K.; Mitragotri, S. Making polymeric micro-and nanoparticles of complex shapes. *Proc. Natl. Acad. Sci. U.S.A.* **2007**, *104*, 11901−11904.
(11) Yoo, J.-W.; Mitragotri, S. Polymer particles that switch shape in response to a stimulus. *Proc. Natl. Acad. Sci. U.S.A.* **2010**, *107*, 11205−11210.
(12) Yabu, H.; Higuchi, T.; Shimomura, M. Unique Phase-Separation Structures of Block-Copolymer Nanoparticles. *Adv. Mater.* **2005**, *17*, 2062−2065.
(13) Perry, J. L.; Herlihy, K. P.; Napier, M. E.; DeSimone, J. M. PRINT: A Novel Platform Toward Shape and Size Specific Nanoparticle Theranostics. *Acc. Chem. Res.* **2011**, *44*, 990−998.
(14) Motornov, M.; Roiter, Y.; Tokarev, I.; Minko, S. Stimuli-responsive nanoparticles, nanogels and capsules for integrated multifunctional intelligent systems. *Prog. Polym. Sci.* **2010**, *35*, 174−211.
(15) Cushen, J. D.; Otsuka, I.; Bates, C. M.; Halila, S.; Fort, S.; Rochas, C.; Easley, J. A.; Rausch, E. L.; Thio, A.; Borsali, R.; Willson, C. G.; Ellison, C. J. Oligosaccharide/Silicon-Containing Block Copolymers with 5 nm Features for Lithographic Applications. *ACS Nano* **2012**, *6*, 3424−3433.
(16) Cushen, J. D.; Bates, C. M.; Rausch, E. L.; Dean, L. M.; Zhou, S. X.; Willson, C. G.; Ellison, C. J. Thin Film Self-Assembly of Poly(trimethylsilylstyrene-b-d,l-lactide) with Sub-10 nm Domains. *Macromolecules* **2012**, *45*, 8722−8728.
(17) Batrakova, E. V.; Kabanov, A. V. Pluronic block copolymers: Evolution of drug delivery concept from inert nanocarriers to biological response modifiers. *J. Controlled Release* **2008**, *130*, 98−106.
(18) Blanazs, A.; Armes, S. P.; Ryan, A. J. Self-Assembled Block Copolymer Aggregates: From Micelles to Vesicles and their Biological Applications. *Macromol. Rapid Commun.* **2009**, *30*, 267−277.
(19) Tyrrell, Z. L.; Shen, Y.; Radosz, M. Fabrication of micellar nanoparticles for drug delivery through the self-assembly of block copolymers. *Prog. Polym. Sci.* **2010**, *35*, 1128−1143.
(20) Miyata, K.; Christie, R. J.; Kataoka, K. Polymeric micelles for nano-scale drug delivery. *React. Funct. Polym.* **2011**, *71*, 227−234.
(21) Robb, M. J.; Connal, L. A.; Lee, B. F.; Lynd, N. A.; Hawker, C. J. Functional block copolymer nanoparticles: toward the next generation of delivery vehicles. *Polym. Chem.* **2012**, *3*, 1618−1628.
(22) Conte, C.; Costabile, G.; d'Angelo, I.; Pannico, M.; Musto, P.; Grassia, G.; Ialenti, A.; Tirino, P.; Miro, A.; Ungaro, F.; Quaglia, F. Skin transport of PEGylated poly(e-caprolactone) nanoparticles assisted by (2-hydroxypropyl)-Ã-cyclodextrin. *J. Colloid Interface Sci.* **2015**, *454*, 112−120.
(23) Jelonek, K.; Li, S.; Wu, X.; Kasperczyk, J.; Marcinkowski, A. Self-assembled filomicelles prepared from polylactide/poly(ethylene glycol) block copolymers for anticancer drug delivery. *Int. J. Pharm.* **2015**, *485*, 357−364.
(24) Nolles, A.; Westphal, A. H.; de Hoop, J. A.; Fokkink, R. G.; Kleijn, J. M.; van Berkel, W. J. H.; Borst, J. W. Encapsulation of GFP in Complex Coacervate Core Micelles. *Biomacromolecules* **2015**, *16*, 1542−1549.
(25) Li, Y.; Bastakoti, B. P.; Yamauchi, Y. Smart Soft-Templating Synthesis of Hollow Mesoporous Bioactive Glass Spheres. *Chem.—Eur. J.* **2015**, *21*, 8038−8042.
(26) Hamley, I. W. Nanostructure fabrication using block copolymers. *Nanotechnology* **2003**, *14*, R39.
(27) Park, C.; Yoon, J.; Thomas, E. L. Enabling nanotechnology with self assembled block copolymer patterns. *Polymer* **2003**, *44*, 6725−6760.
(28) Broz, P.; Driamov, S.; Ziegler, J.; Ben-Haim, N.; Marsch, S.; Meier, W.; Hunziker, P. Toward Intelligent Nanosize Bioreactors: A pH-Switchable, Channel-Equipped, Functional Polymer Nanocontainer. *Nano Lett.* **2006**, *6*, 2349−2353.
(29) Mai, Y.; Eisenberg, A. Self-assembly of block copolymers. *Chem. Soc. Rev.* **2012**, *41*, 5969−5985.
(30) Schacher, F. H.; Rupar, P. A.; Manners, I. Functional Block Copolymers: Nanostructured Materials with Emerging Applications. *Angew. Chem., Int. Ed.* **2012**, *51*, 7898−7921.
(31) Higuchi, T.; Tajima, A.; Yabu, H.; Shimomura, M. Spontaneous formation of polymer nanoparticles with inner micro-phase separation structures. *Soft Matter* **2008**, *4*, 1302−1305.
(32) Higuchi, T.; Tajima, A.; Motoyoshi, K.; Yabu, H.; Shimomura, M. Suprapolymer Structures from Nanostructured Polymer Particles. *Angew. Chem., Int. Ed.* **2009**, *48*, 5125−5128.
(33) Hirai, Y.; Wakiya, T.; Yabu, H. Virus-like particles composed of sphere-forming polystyrene-block-poly(t-butyl acrylate) (PS-b-PtBA) and control of surface morphology by homopolymer blending. *Polym. Chem.* **2017**, *8*, 1754−1759.
(34) Avalos, E.; Higuchi, T.; Teramoto, T.; Yabu, H.; Nishiura, Y. Frustrated phases under three-dimensional confinement simulated by a set of coupled Cahn-Hilliard equations. *Soft Matter* **2016**, *12*, 5905−5914.
(35) LeGrand, D. G. *Encyclopedia of Polymer Science and Technology*; John Wiley & Sons, Inc., 2011.

DOI: 10.1021/acsomega.7b01557
ACS Omega 2018, 3, 1304−1314

(36) Majewski, P. W.; Yager, K. G. Rapid ordering of block copolymer thin films. *J. Phys.: Condens. Matter* **2016**, *28*, 403002.
(37) Higuchi, T.; Motoyoshi, K.; Sugimori, H.; Jinnai, H.; Yabu, H.; Shimomura, M. Phase Transition and Phase Transformation in Block Copolymer Nanoparticles. *Macromol. Rapid Commun.* **2010**, *31*, 1773−1778.
(38) Higuchi, T.; Shimomura, M.; Yabu, H. Reorientation of Microphase-Separated Structures in Water-Suspended Block Copolymer Nanoparticles through Microwave Annealing. *Macromolecules* **2013**, *46*, 4064−4068.
(39) Cavicchi, K. A.; Russell, T. P. Solvent Annealed Thin Films of Asymmetric Polyisoprene-Polylactide Diblock Copolymers. *Macromolecules* **2007**, *40*, 1181−1186.
(40) Zhang, X.; Harris, K. D.; Wu, N. L. Y.; Murphy, J. N.; Buriak, J. M. Fast Assembly of Ordered Block Copolymer Nanostructures through Microwave Annealing. *ACS Nano* **2010**, *4*, 7021−7029.
(41) Qiang, Z.; Ye, C.; Lin, K.; Becker, M. L.; Cavicchi, K. A.; Vogt, B. D. Evolution in surface morphology during rapid microwave annealing of PS-b-PMMA thin films. *J. Polym. Sci., Part B: Polym. Phys.* **2016**, *54*, 1499−1506.
(42) Ku, K. H.; Shin, J. M.; Kim, M. P.; Lee, C.-H.; Seo, M.-K.; Yi, G.-R.; Jang, S. G.; Kim, B. J. Size-Controlled Nanoparticle-Guided Assembly of Block Copolymers for Convex Lens-Shaped Particles. *J. Am. Chem. Soc.* **2014**, *136*, 9982−9989.
(43) Jang, S. G.; Audus, D. J.; Klinger, D.; Krogstad, D. V.; Kim, B. J.; Cameron, A.; Kim, S.-W.; Delaney, K. T.; Hur, S.-M.; Killops, K. L.; Fredrickson, G. H.; Kramer, E. J.; Hawker, C. J. Striped, Ellipsoidal Particles by Controlled Assembly of Diblock Copolymers. *J. Am. Chem. Soc.* **2013**, *135*, 6649−6657.
(44) Lee, J.; Ku, K. H.; Kim, M.; Shin, J. M.; Han, J.; Park, C. H.; Yi, G.-R.; Jang, S. G.; Kim, B. J. Stimuli-Responsive, Shape-Transforming Nanostructured Particles. *Adv. Mater.* **2017**, *29*, 1700608.
(45) Ku, K. H.; Yang, H.; Shin, J. M.; Kim, B. J. Aspect ratio effect of nanorod surfactants on the shape and internal morphology of block copolymer particles. *J. Polym. Sci., Part A: Polym. Chem.* **2015**, *53*, 188−192.
(46) Jeon, S.-J.; Yi, G.-R.; Koo, C. M.; Yang, S.-M. Nanostructures Inside Colloidal Particles of Block Copolymer/Homopolymer Blends. *Macromolecules* **2007**, *40*, 8430−8439.
(47) Jeon, S.-J.; Yi, G.-R.; Yang, S.-M. Cooperative Assembly of Block Copolymers with Deformable Interfaces: Toward Nanostructured Particles. *Adv. Mater.* **2008**, *20*, 4103−4108.
(48) Schmidt, B. V. K. J.; Elbert, J.; Scheid, D.; Hawker, C. J.; Klinger, D.; Gallei, M. Metallopolymer-Based Shape Anisotropic Nanoparticles. *ACS Macro Lett.* **2015**, *4*, 731−735.
(49) Klinger, D.; Wang, C. X.; Connal, L. A.; Audus, D. J.; Jang, S. G.; Kraemer, S.; Killops, K. L.; Fredrickson, G. H.; Kramer, E. J.; Hawker, C. J. A Facile Synthesis of Dynamic, Shape-Changing Polymer Particles. *Angew. Chem., Int. Ed.* **2014**, *53*, 7018−7022.
(50) Yang, H.; Ku, K. H.; Shin, J. M.; Lee, J.; Park, C. H.; Cho, H.-H.; Jang, S. G.; Kim, B. J. Engineering the Shape of Block Copolymer Particles by Surface-Modulated Graphene Quantum Dots. *Chem. Mater.* **2016**, *28*, 830−837.
(51) Deng, R.; Liu, S.; Liang, F.; Wang, K.; Zhu, J.; Yang, Z. Polymeric Janus Particles with Hierarchical Structures. *Macromolecules* **2014**, *47*, 3701−3707.
(52) McKenzie, B. E.; de Visser, J. F.; Friedrich, H.; Wirix, M. J. M.; Bomans, P. H. H.; de With, G.; Holder, S. J.; Sommerdijk, N. A. J. M. Bicontinuous Nanospheres from Simple Amorphous Amphiphilic Diblock Copolymers. *Macromolecules* **2013**, *46*, 9845−9848.
(53) Li, L.; Matsunaga, K.; Zhu, J.; Higuchi, T.; Yabu, H.; Shimomura, M.; Jinnai, H.; Hayward, R. C.; Russell, T. P. Solvent-Driven Evolution of Block Copolymer Morphology under 3D Confinement. *Macromolecules* **2010**, *43*, 7807−7812.
(54) Fan, H.; Jin, Z. Selective Swelling of Block Copolymer Nanoparticles: Size, Nanostructure, and Composition. *Macromolecules* **2014**, *47*, 2674−2681.
(55) Deng, R.; Liang, F.; Li, W.; Yang, Z.; Zhu, J. Reversible Transformation of Nanostructured Polymer Particles. *Macromolecules* **2013**, *46*, 7012−7017.
(56) Shin, J. M.; Kim, Y.; Yun, H.; Yi, G.-R.; Kim, B. J. Morphological Evolution of Block Copolymer Particles: Effect of Solvent Evaporation Rate on Particle Shape and Morphology. *ACS Nano* **2017**, *11*, 2133−2142.
(57) Connal, L. A.; Lynd, N. A.; Robb, M. J.; See, K. A.; Jang, S. G.; Spruell, J. M.; Hawker, C. J. Mesostructured Block Copolymer Nanoparticles: Versatile Templates for Hybrid Inorganic/Organic Nanostructures. *Chem. Mater.* **2012**, *24*, 4036−4042.
(58) Toyota, T.; Tsuha, H.; Yamada, K.; Takakura, K.; Yasuda, K.; Sugawara, T. Fluorescence Microscopic Investigation on Morphological Changes of Giant Multilamellar Vesicles Induced by Amphiphilic Additives. *Langmuir* **2006**, *22*, 1976−1981.
(59) Ohta, T.; Ito, A. Dynamics of phase separation in copolymer-homopolymer mixtures. *Phys. Rev. E: Stat. Phys., Plasmas, Fluids, Relat. Interdiscip. Top.* **1995**, *52*, 5250−5260.
(60) Teramoto, T. Three-Dimensional Morphology in Copolymer-Homopolymer Mixtures. *J. Phys. Soc. Jpn.* **2001**, *70*, 3217−3220.
(61) Teramoto, T.; Nishiura, Y. Double Gyroid Morphology in a Gradient System with Nonlocal Effects. *J. Phys. Soc. Jpn.* **2002**, *71*, 1611−1614.
(62) Koizumi, S.; Hasegawa, H.; Hashimoto, T. Ordered Structures of Block Copolymer/Homopolymer Mixtures. 5. Interplay of Macro- and Microphase Transitions. *Macromolecules* **1994**, *27*, 6532−6540.
(63) Ohta, T.; Kawasaki, K. Equilibrium morphology of block copolymer melts. *Macromolecules* **1986**, *19*, 2621−2632.
(64) Nishiura, Y.; Ohnishi, I. Some mathematical aspects of the micro-phase separation in diblock copolymers. *Phys. D* **1995**, *84*, 31−39.
(65) Helfand, E.; Tagami, Y. Theory of the interface between immiscible polymers. *J. Polym. Sci., Part B: Polym. Lett.* **1971**, *9*, 741−746.
(66) Helfand, E.; Tagami, Y. Theory of the Interface between Immiscible Polymers. II. *J. Chem. Phys.* **1972**, *56*, 3592−3601.
(67) Zeman, L.; Patterson, D. Effect of the Solvent on Polymer Incompatibility in Solution. *Macromolecules* **1972**, *5*, 513−516.
(68) Longanecker, M.; Modi, A.; Dobrynin, A.; Kim, S.; Yuan, G.; Jones, R.; Satija, S.; Bang, J.; Karim, A. Reduced Domain Size and Interfacial Width in Fast Ordering Nanofilled Block Copolymer Films by Direct Immersion Annealing. *Macromolecules* **2016**, *49*, 8563−8571.
(69) Eyre, D. *An Unconditionally Stable One-Step Scheme for Gradient Systems, in Computational and Mathematical Models of Microstructural Evolution*; Bullard, K., Stoneham, C., Eds.; MRS, 1998.
(70) Teramoto, T.; Nishiura, Y. Morphological characterization of the diblock copolymer problem with topological computation. *Jpn. J. Ind. Appl. Math.* **2010**, *27*, 175−190.

DOI: 10.1021/acsomega.7b01557
ACS Omega 2018, 3, 1304−1314